

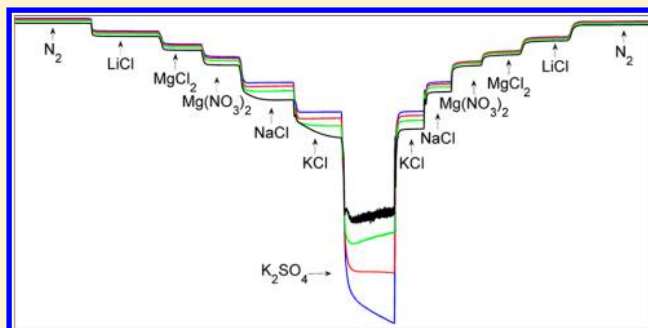
Water Sorption and Glass Transition of Pig Gastric Mucin Studied by QCM-D

Yana Znamenskaya, Javier Sotres, Sergei Gavryushov,[†] Johan Engblom, Thomas Arnebrant, and Vitaly Kocherbitov*

Biomedical Science, Faculty of Health and Society, Malmö University, SE-205 06 Malmö, Sweden

S Supporting Information

ABSTRACT: Hydration of films of pig gastric mucin was studied using a quartz crystal microbalance with dissipation monitoring (QCM-D) equipped with a humidity module. As a prerequisite, the water adsorption isotherm of a clean silica surface was determined. Atomic force microscopy was used to characterize the changes occurring on the silica surface after repeated sorption/desorption and cleaning cycles. The water sorption isotherms of several hundreds of nanometers thick mucin films were obtained in QCM-D experiments using analysis of overtone behavior. The results show that the sorption isotherms are not dependent on the film thicknesses and are in good agreement with sorption calorimetric data on mucin in the bulk phase. Moreover, hydration-induced changes of rheological properties of mucin films were investigated using a model-free approach. The ratio of G'/G'' was evaluated as a function of relative humidity. The transition from solidlike behavior to liquidlike behavior was observed in the same humidity range as in sorption calorimetric experiments. Thus, ability of QCM-D to monitor glass transition in biopolymers was demonstrated.



1. INTRODUCTION

Mucus is a complex viscous adherent secretion¹ that covers the luminal surface of the gastrointestinal (GI), respiratory, urogenital, and eye tissues, as well as the peritoneal surface of intra-abdominal organs in humans and most mammals.² The functions of mucus differ from one source to another but generally it is responsible for protection and transportation.^{1–4} Mucus is also known for its water-based lubrication properties.^{5,6} Mucus consists of water (95%), salts, lipids, and proteins. But the main component which is responsible for its viscoelastic properties is the glycoprotein mucin.¹ Mucins are large macromolecules with a molecular weight ranging from 0.5 to 20–40 MDa.^{1,7} The mucin molecules consist of a polypeptide backbone, polysaccharide side chains, cysteine-rich domains, and N- and C- terminal ends.⁸ The carbohydrate content can be up to 80% of the total mass of the molecule,¹ and it depends on the location of the mucous secretion. For example, for pig gastric mucin (PGM) the carbohydrate content is 86%, for bovine submaxillary gland mucin (BSM) it is 69%.⁹ Due to the complexity of the mucin molecule, it has been described by different models ranging from fiberlike^{1,5,7,10} to dumbbell^{10–12} structures. Mucin phase behavior has been studied using different techniques^{5,10,13–18} including polarized light microscopy,^{5,15,16} small-angle neutron scattering (SANS),¹⁷ differential scanning calorimetry (DSC),⁵ and sorption calorimetry.¹⁰ It has been shown that the phase behavior of mucin is dependent on the hydration level¹⁰ and according to some reports mucin can form liquid crystalline

phases.^{15,16} According to several calorimetric studies, mucin systems undergo glass transitions, and the T_g values differ for different types of mucin.^{5,13,17,18} According to our previous work,¹⁰ there are two regions in the phase diagram where the glass transition of PGM is dependent and independent of hydration levels. In particular, at mucin concentrations from 0 to 67 wt %, the glass transition occurs at the same temperature, around $-15\text{ }^{\circ}\text{C}$. At higher concentrations of mucin, T_g increases with increasing mucin concentrations. In living systems, mucins are most often arranged in thin films covering the hydrated tissues. Hydration of mucin films and not of the bulk material therefore plays the key role in the protection of the tissues against dehydration.

The objective of this work is to study hydration-induced rheological changes and glass transition behavior of mucin in thin films, which to the best of our knowledge have not been studied before. Hydration of PGM films at different relative humidity levels is studied using a quartz crystal microbalance with dissipation monitoring (QCM-D) and compared with the results of sorption calorimetric data¹⁰ on hydration of bulk mucin. QCM-D together with the humidity module allows measuring a water sorption isotherm and monitoring rheological properties of relatively thin films using very small amounts of samples. Studies on hydration/dehydration of

Received: December 5, 2012

Revised: January 22, 2013

Published: January 31, 2013

biopolymer films obtained by QCM-D are rarely reported in the literature. To our best knowledge, there are only a few reports that compare water sorption isotherms obtained using QCM-D with experimental data obtained using other techniques.^{19–21} Furthermore, agreement between QCM-D water sorption isotherms and the data obtained by other techniques²⁰ is not always good. In some cases, sorption isotherms studied by QCM-D are compared not with experimental data but with theoretical sorption models.^{22–24} For example, experimentally obtained sorption isotherms of lysozyme²² were compared with the results of calculations from the D'Arcy–Watt model²⁵ or QCM-D data were fitted using the Langmuir sorption isotherm.²³ In this work, based on the analysis of overtone behavior, we obtained a QCM-D water sorption isotherm of mucin that is in good agreement with the sorption calorimetric water sorption isotherm of the same biopolymer. Moreover, for the first time, we demonstrate that hydration-induced glass transition in biopolymer films can be studied using QCM-D. The obtained glass transition data are in good agreement with previously published sorption calorimetric results.

2. MATERIALS AND METHODS

Mucin. Commercially available, partially purified PGM type III, containing 0.5–1.5% bound sialic acid (Sigma, USA; cat. no. M1778, lot no. 018K7001) was purchased from Sigma. PGM was dried in vacuum at room temperature in contact with 3 Å molecular sieves for 24–48 h directly before mixing with water.

The stock solution with mucin concentration of 1 wt % was prepared and equilibrated for 24 h. After that the stock solution (1 wt % of mucin) was diluted to the concentration of 0.20–0.22 wt %. Ultra-high-quality (UHQ) water, purified at 25 °C by Elgastat UHQ II Model UHQ-PS-MK3 (Elga Ltd., High Wycombe, Bucks, UK), was used as a solvent.

Drop Coating. The drop coating process was used as deposition method. PGM films were prepared from the mucin solution of 0.20–0.22 wt %. A drop of PGM solution was deposited onto the QCM sensor silica surface and left for solvent evaporation in a desiccator with silica gel at room temperature. It is important that the complete surface is covered by drop, and all calculations done over the whole surface. The surface area of the sensor is equal to 153.9 mm². The roughness of the samples was estimated from 5 μm × 5 μm AFM images, obtaining a surface area difference value (SAD, see definition below) of 2.6 ± 0.2%.

Saturated Salt Solutions. Six different saturated salt solutions for setting up different relative humidity (RH) levels²⁶ were prepared. The following salts were mixed in excess with water to form saturated solutions: LiCl, MgCl₂, Mg(NO₃)₂, NaCl, KCl, and K₂SO₄. After that, the salt solutions were equilibrated during 2–3 weeks, and then filtered and used in experiments. The humidities of those solutions were verified using a hygrometer and for each saturated salt solution according to the literature²⁶ they are as follows: 11.3% (LiCl), 32.8% (MgCl₂), 52.9% (Mg(NO₃)₂), 75.3% (NaCl), 84.3% (KCl), and 97.3% (K₂SO₄).

QCM-D. A quartz crystal microbalance with dissipation monitoring, QCM-D, Q-sense E4, together with a Q-sense humidity module, QHM 401, was used to characterize the hydration of the PGM films. QCM-D measurements were performed on AZ-cut 5 MHz quartz crystals (sensors) purchased from Biolin Scientific AB, Västra Frölunda, Sweden.

Sensors with a silica surface (QX3 303 silicon dioxide, 50 nm) were used. Silica surfaces were cleaned with water and ethanol followed by plasma cleaning for 10 min in low-pressure residual air using a radio frequency glow discharge unit (Plasma Cleaner PDC-32 G, Harrick Scientific, Ossining, NY).

The humidity module contains a Gore membrane which separates the sensor from the liquid. QCM-D allows frequency and dissipation changes to be measured at the same time.²⁷ Knowing the frequency and dissipation changes, the mass and the thickness of film can be calculated. The thickness of the film was calculated assuming the density of mucin²⁸ is equal to 1080 kg m⁻³. The obtained raw data were evaluated using Q-tools software (Q-sense AB) and MATLAB. PGM film was scratched with AFM to estimate a thickness of the film. The values of the thickness obtained by QCM-D and AFM had the same order of magnitude.

The drop-coated sensor with PGM film was placed into the humidity module. To get as low humidity inside the chamber as possible, the module together with the coated sensor was dried further in a desiccator with silica gel under vacuum at room temperature during 1 h. After that QCM-D measurements were immediately started. The fundamental as well as the overtone frequencies were determined. Then the chamber was circulated with dry N₂ to achieve 0% RH. After that, salt solutions were pumped through the module with an Ismatec peristaltic pump, IPC-N 4, at a speed of 100 μL/min. The sorption experiments started at the lowest RH (11.3%) with further increasing RH (32.8, 52.9, 75.3, 84.3, and 97.3%). After that, desorption was done in the reverse order.

In addition, QCM-D measurements were performed on a SiO₂ sensor without PGM film. The experimental procedure was the same as with the coated sensor. In this case, adsorption of water on the silica surface was studied. The obtained raw data were evaluated using Q-tools software (Q-sense AB) and MATLAB.

AFM. The PGM films and the underlying SiO₂ sensors were examined with a commercial atomic force microscope (AFM) equipped with a liquid cell (MultiMode 8 SPM with a NanoScope V control unit, Bruker AXS). Triangular silicon nitride cantilevers with nominal spring constant 0.7 N·m⁻¹ were employed (ScanAsyst-Fluid, Bruker AXS). The samples were imaged in air, at room temperature, by operating the AFM in the peak force tapping mode. Analysis and processing of AFM images were performed with the WSxM software.²⁹ The roughness of the AFM images was quantified through the surface area difference parameter, SAD, defined as SAD = (surface area – projected area)/(projected area) × 100.

The mucin film was scratched with the AFM in order to estimate its thickness. For this, an area of the sample (2 μm × 2 μm) was scratched (further details can be found in ref 30). The surface charge density of the SiO₂ sensors was probed in 1 mM NaCl by performing normal force measurements with rectangular silicon nitride cantilevers (nominal spring constant of 0.5 N·m⁻¹, OMLC-RC800PSA, Olympus). Analysis and processing of force measurements were performed in MATLAB (The MathWorks, Inc., MA).

3. RESULTS AND DISCUSSION

Adsorption of Water on the SiO₂ Sensor. Before analyzing the sorption isotherm of the biopolymer deposited on SiO₂, one needs to evaluate the contribution of the sensor itself to the amount of the adsorbed water. Therefore, QCM-D measurements were performed on clean SiO₂ sensor at 25 °C

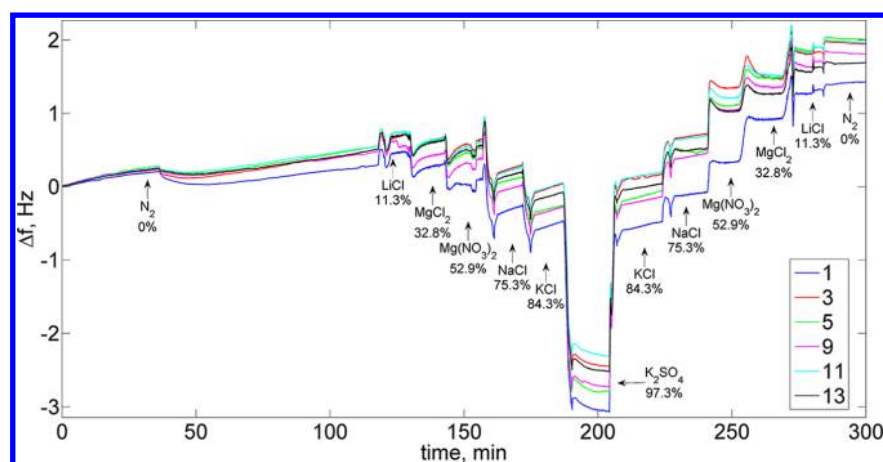


Figure 1. Change of frequency (Δf) vs time upon water sorption/desorption onto the hydrophilic silica surface. Numbers of overtones are presented in the legend. Salts and corresponding RHs are shown in the figure.

to study the water adsorption/desorption on the silica surface. The change of frequency versus time during water adsorption/desorption on the silica surface is presented in Figure 1. The stepwise changes in frequencies correspond to each hydration/dehydration level. Figure 1 shows the small changes in frequency during the experiment. The mass of the water film was calculated using the Sauerbrey³¹ equation, where the linear relationship between mass addition and frequency shift is described

$$\frac{\Delta f}{n} = -\frac{2mf_0^2}{z_q} \quad (1)$$

where $(\Delta f)/n$ is the frequency change normalized to the overtone number n , $Z_q = 8.8 \times 10^6 \text{ kg m}^{-2} \text{ s}^{-1}$ is the acoustic or mechanical impedance of quartz, f_0 is the fundamental frequency, and m is the mass in kg m^{-2} .

The mass shifts at each RH with respect to the previous RH level were determined for each overtone. The determined mass shifts were summed up at each RH to obtain total cumulative mass. The thickness of the adsorbed water layer was calculated using the following equation, where the thickness t is proportional to the adsorbed volume V

$$t = \frac{V}{A} = \frac{m}{A\rho} \quad (2)$$

where m/A is the Sauerbrey mass and ρ is the density of water. For each RH level the thicknesses have been determined for all overtones, and then the mean values of thicknesses were used in the adsorption isotherm plot (Figure 2). The adsorption isotherms of water on SiO_2 obtained in several experiments are shown in Figure 2, and the experimental results are compared with literature data on the t -curve for water on silica surface.³² The adsorption isotherms have similar shapes, which demonstrates that very small thicknesses, such as water monolayer thickness, can be determined using QCM-D. On the other hand, the thicknesses of adsorbed water layers at low RH levels differ between our experimental data and the literature data.³² A possible explanation is that despite all taken measures, the chamber was not completely dry in the beginning of the experiment, which affected the amount of adsorbed water on silica surface. Furthermore, experimental and literature data are obtained on different silica surfaces and hence have different

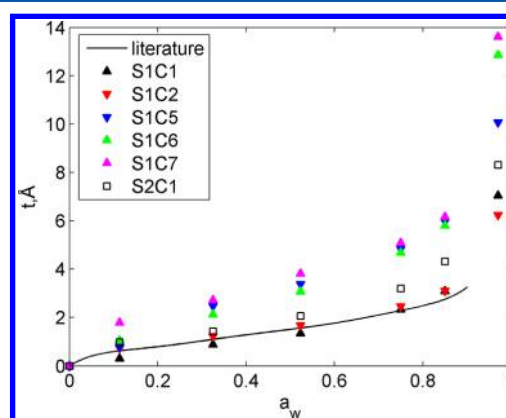


Figure 2. Dependence of the thickness of the adsorbed water layer on the water activity. Triangles and squares are experimental data (mean value of the thickness) and solid line is literature data.³² Triangles, sensor number 1 (S1), cleaned seven times in total; squares, sensor number 2 (S2), treated one time; C = experimental cycle.

surface roughness, which could explain the discrepancy in the thicknesses of the adsorbed water layer.

During measurements it was noticed that the amount of adsorbed water on the silica surface is dependent on how many times the SiO_2 sensor was used (Figure 2). The experimental cycle (C) included cleaning with water and ethanol followed by plasma cleaning for 10 min, and directly after that water adsorption and desorption experiments. Figure 2 presents the comparison of adsorption isotherms of water on two SiO_2 sensors. On one SiO_2 sensor (S1) experiments were performed seven times in total, and the other SiO_2 sensor (S2) was used only once. The thickness of an adsorbed water layer depending on each cleaning treatment versus water activity is shown in the Figure 2. According to these data, the amount of water adsorbed on the silica surface increases with each experimental cycle. This can be explained either by changes in the surface chemistry with formation of more silanol groups on the SiO_2 sensor or by the changes in the area of the SiO_2 surface due to increased roughness.

The increase of roughness in a sorption–desorption cleaning cycle would imply a decrease of mass of the sensor due to its wear. To investigate this, the dependence of the first overtone frequencies of SiO_2 sensors on the number of experimental cycles has been compared. The data points (not shown) were

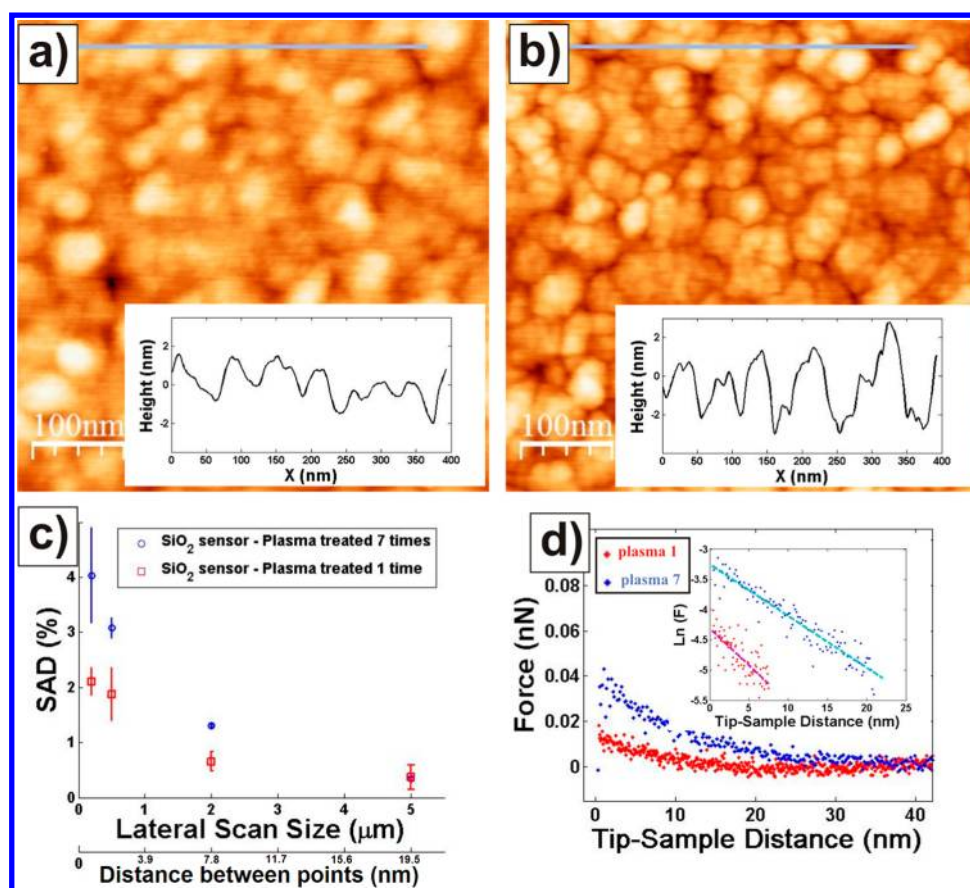


Figure 3. (a,b) Topography images of SiO₂ QCM-D sensors plasma-treated once (a) and seven times (b). Color scale goes from 0 nm (black) to 10 nm (white). Both images include as an inset a cross-sectional profile of the surfaces (locations indicated by blue lines in both images). (c) Surface area difference values for the two different sensors studied in terms of the lateral size of the scan, and of the length interval between adjacent scan points. Data was calculated by averaging roughness values obtained with two different tips. (d) Force vs separation curves obtained with the same tip for the sensors from (a) (red dots) and (b) (blue dots). Each of the curves was obtained by averaging 10 different curves. The inset of the figure shows the same identical data, but in a representation of the natural logarithm of the force vs the separation between tip and sample. Linear fits of these plots are also included as dashed lines.

strongly scattered but indicated that the frequency increased with the number of experimental cycles. An increase of the frequency means a decrease of the mass of the crystal. This result is consistent with changes in roughness of the SiO₂ sensor. The increase in roughness can be the reason for higher adsorption of water on the SiO₂ surface which is treated seven times (S1C7) compared to sensors used only once (S1C1 and S2C1) (Figure 2). For further characterization of the surface properties, the two SiO₂ sensors were examined by the AFM.

AFM. AFM was used to investigate the mechanisms underlying the dependence of the water adsorption on the silica sensor on the number of experimental cycles.

First, two SiO₂ sensors, used in experiments, were visualized in air at room temperature (Figure 3). The topography of the sensor subjected to one experimental cycle is shown in Figure 3a and the topography of the sensor subjected to seven experimental cycles is shown in Figure 3b. From the images it is clear that experimental cycles (that include cleaning treatment) increase the roughness of the SiO₂ surfaces and, therefore, the surface area of the sensors. When measured with AFM, roughness is a quantity that has to be handled with caution. AFM topography images consist of height values acquired with a finite-size probe/tip at distant surface points. Therefore, the lower the separation between adjacent points, the higher the resolution in roughness will be. However, this trend is limited

by the size of the tip, i.e., probing two points separated by a distance much lower than the size of the tip will provide redundant topography information. Figure 3c shows SAD values for the two different sensors calculated from scans of different lateral sizes. The corresponding length intervals between adjacent points are also indicated in the plot. Results reveal that the roughness of the surfaces increases with the number of experimental cycles. Specifically, from the images with the highest resolution, a difference in surface area of ca. 2% is observed between the two studied sensors. While this increase in surface area might not be enough to account for the increase in mass of adsorbed water, it is fair to recall that the true value of the surface area might be hindered by the limit in the lateral achievable resolution established by the AFM tip (nominal effective tip radius of ca. 20 nm). The trend observed in Figure 3c for the dependence of the measured increase in roughness with the lateral resolution of the AFM images suggests that the real increase in surface area originated from additional experimental cycles may be considerably higher. This makes us believe that the increase in the surface area is the reason behind the increase in mass of adsorbed water with the number of experimental cycles.

Also, two SiO₂ sensors were studied to see if experimental cycles induce any changes in the surface chemistry of the sensors. For this, the same two sensors, used for topography

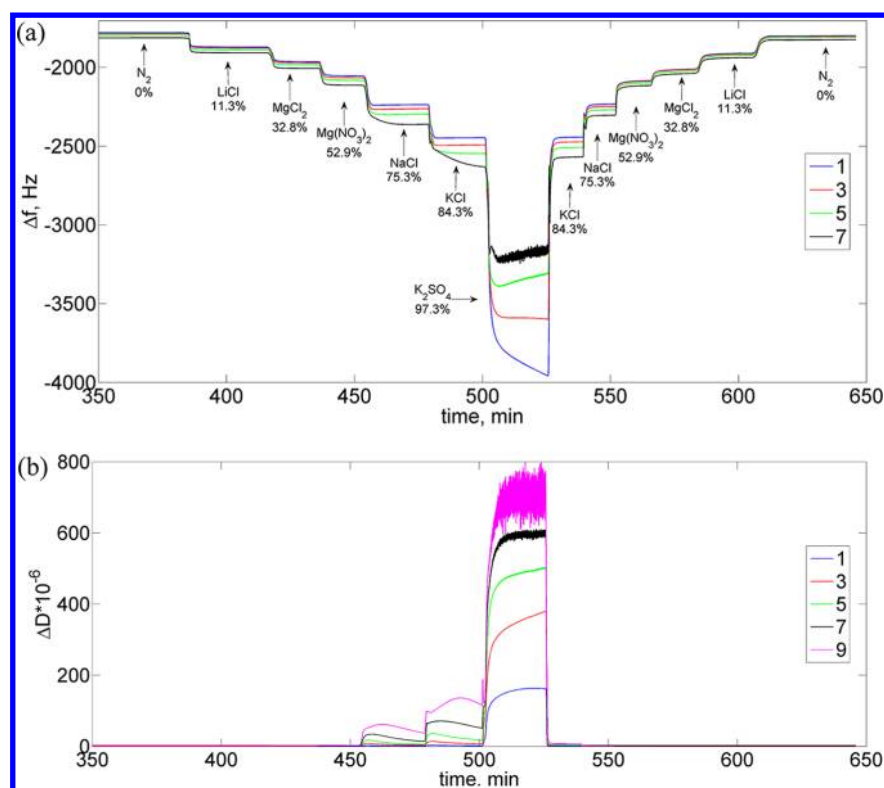


Figure 4. Sorption/desorption of water by 262 nm PGM film. (a) Changes in frequency vs time for different overtones during sorption/desorption processes. The frequency change normalized to overtone number of coated SiO_2 sensor with respect to uncoated sensor is presented. (b) Dissipation change vs time for different overtones during sorption/desorption processes.

studies, were immersed in a 1 mM NaCl solution and the normal force developed between the sensors and a silicon nitride tip was probed. In this situation, an electrical double layer (EDL) force will develop between tip and sample. If the tip is considered as a sphere, the sample as a plane, and small separations ($d \leq 2$ nm) where van der Waals interaction will dominate are not considered, it is fair to approximate the EDL force exerted on the AFM tip, F_{EDL} , as an exponential function of the tip–sample separation, d , of the form³³

$$F_{\text{EDL}}(d) = \frac{4\pi R_t \sigma_t \sigma_s \lambda_D}{\epsilon \epsilon_0} e^{-d/\lambda_D} \quad (3)$$

where R_t is the effective tip radius, ϵ is the dielectric constant of the medium, ϵ_0 the permittivity of vacuum, σ_t and σ_s are the surface charge densities of tip and sample, and λ_D , also known as the Debye length, is the decay length of the interaction. λ_D depends on the ionic strength of the solution, but not on the surface chemistry (charge density) of the interacting surfaces. For 1 mM NaCl aqueous solution λ_D is ca. 9.6 nm. Figure 3d shows force versus separation curves obtained with the same tip for the two different sensors studied. Each of the represented curves is the average of 10 different curves. The inset in Figure 3d shows the same data, but in a representation of the natural logarithm of the force versus the separation between tip and sample. This proves the exponential dependence of the force, and therefore its EDL origin, as the logarithm of an exponentially decaying force should decay linearly with a slope equal to the inverse of the characteristic length of the interaction (λ_D in this case). Fits of the curves to an exponentially decaying function provide an EDL force amplitude, $F_{\text{EDL}}^0(1) = 0.015 \pm 0.005$ nN, and a decay length, $\lambda_D(1) = 8.1 \pm 1.0$ nm for the sensor used once (S2C1). For the

sensor used seven times in measurements (S1C7) the values are $F_{\text{EDL}}^0(7) = 0.038 \pm 0.012$ nN and $\lambda_D(1) = 12.2 \pm 2.6$ nm. Considering the different approximations assumed when modeling the EDL force with an exponential function,³³ a reasonable agreement is found between the expected and the experimentally obtained λ_D values. While parameters such as R_t and σ_t are difficult to estimate, it is easier to estimate the change in surface charge density since the same tip was used for both experiments $F_{\text{EDL}}^0(7)/F_{\text{EDL}}^0(1) = \sigma_7/\sigma_1 = 2.5 \pm 1.2$. Thus, the surface charge density of the sensor measured seven times (S1C7) was ca. 2.5 times higher than that of the sensor used only once (S2C1). One should stress that the surface charge density here is the number of charges per projected area and not per real surface area. Therefore, the increase of the surface charge is consistent with the increase in roughness. The observed force ratio is close to the ratio of masses of water in the adsorption experiments (Figure 2). Thus, combined evidence from QCM frequency analysis, from AFM topography in air, and from analysis of forces in liquid suggests that the increase of adsorbed amount of water after sorption–desorption–cleaning cycles is caused by an increase in roughness of the silica surface.

Figure 2 shows that only small amounts of water are adsorbed on silica surfaces. If the studied film is relatively thin, then such small amounts of the adsorbed water on silica surface should be taken into account, and the water–sensor interactions become important in the sorption experiments. Figure 2 demonstrates that the obtained thicknesses are small (typically below 1 nm) compared to those of PGM films (see below), and the amount of water adsorbed at the silica surface does not affect the thickness of PGM film. Hence the water–

sensor interactions can be ignored in the study of the hydration of mucin presented below.

Sensor Coated with PGM Film. Sorption/desorption of water by PGM films have been analyzed using QCM-D equipped with Q-Sense humidity module.

First, different thicknesses of the PGM films, ranging from 16 nm to 2.5 μm , were examined at 0% humidity. To achieve 0% humidity, the chamber was circulated with dry N_2 . The dry film of PGM behaves as a solid and therefore its mass was calculated using the Sauerbrey³¹ equation that describes a linear relationship between added mass and a frequency shift (eq 1). For calculation of the dry film mass m_d , the frequency changes upon loading the sensor with dry PGM Δf_d for all overtones were used

$$\frac{\Delta f_d}{n} = -am_d \quad (4)$$

where $a = (2f_0^2)/z_q$ from eq 1. After the dry film masses from each overtone data were calculated, the mean value of dry PGM film mass \bar{m}_d was used in further calculations. The thickness of the PGM film was calculated using eq 2.

PGM films of thicknesses around 180–710 nm were chosen for presentation in this work. The reason for that is the following: in the case of thin films, values of frequency shifts normalized per overtone number $(\Delta f)/n$ did not show any pronounced dependence on the overtone number. When the thicknesses of the PGM films were large, more than 1 μm , the results were unstable and overtones started to disappear. Thus, such thicknesses were not used in further experiments.

A QCM-D experiment of sorption/desorption of water for a 262 nm PGM film on silica surface is shown in Figure 4. The frequency change normalized to overtone number of the coated SiO_2 sensor with respect to uncoated sensor is presented in Figure 4a. A large frequency shift with respect to empty sensor is observed when PGM coating is applied on the sensor. Hence the frequency shifts normalized to the overtone number $(\Delta f)/n$ shown in Figure 4a start from values around -2000 Hz which corresponds to the dry PGM film. The stepwise changes in frequencies are associated with each hydration/dehydration level. Figure 4a shows that the frequencies decrease with increasing humidity in the sorption experiment, whereas in the later part of the experiment they increase during the desorption process. The PGM film mass returned to the previous values corresponding to each RH level, when the humidity was changed from 97.3% back to 11.3%. Hence hysteresis of frequencies and masses of water adsorbed by PGM film in sorption/desorption experiments was not observed.

Changes in dissipation at each RH level are presented in Figure 4b. It is shown that dissipation is only slightly changed at low RH levels (Figure S1 in the Supporting Information). Large changes in dissipation take place at high hydration/dehydration levels.

Sorption Isotherm. The data on the frequency change normalized to overtone number of coated SiO_2 sensor with respect to uncoated sensor were analyzed using the equation for a single viscoelastic film³⁴ in air, where the frequency shift $(\Delta f)/n$ is proportional to the square of the overtone order n^2

$$\frac{\Delta f}{n} = \frac{-2f_0^2 m_f}{Z_q} \left(1 + \frac{1}{3} \frac{Z_q^2}{Z_f^2} \left(\frac{m_f}{m_q} n \pi \right)^2 \right) \quad (5)$$

where $Z_q = 8.8 \times 10^6 \text{ kg m}^{-2} \text{ s}^{-1}$ is the acoustic or mechanical impedance of quartz; $Z_f = (\rho(G' + G''))^{1/2}$ is the acoustic impedance of the film; f_0 is the fundamental frequency; m_f is the mass of the film per unit area; and m_q is the areal mass density of the crystal.

Equation 5 can be presented in the following way

$$\frac{\Delta f}{n} = -am_f(1 + bm_f^2 n^2) \quad (6)$$

where $a = (2f_0^2)/z_q$ and $b = (1/3)[(z_q^2 \pi^2)/(z_f^2 m_q^2)]$.

If the data are extrapolated to the zero overtone, then the frequency shift $(\Delta f)/n$ is proportional to the film mass m_f . Thus, extrapolation to the zero overtone at each RH level gives a frequency change which is proportional to the mass of PGM film.

The frequency change proportional to the mass of the water absorbed by the PGM film was calculated for each overtone at each RH level as follows:

$$\frac{\Delta f_w}{n} = \frac{\Delta f}{n} - \frac{\Delta f_d}{n} \quad (7)$$

After all simplifications (see derivation in Section SI in the Supporting Information), data on calculated mass of water absorbed by PGM film were normalized to the dry mass of PGM film \bar{m}_d

$$\frac{m_w^s}{\bar{m}_d} = \frac{m_w}{\bar{m}_d} + b \frac{m_f^3}{\bar{m}_d} n^2 \quad (8)$$

and extrapolated to the zero overtones for each RH level, where m_w^s is the formal mass of the water absorbed by the PGM film calculated by the Sauerbrey equation and m_w is the real mass of the water absorbed by the PGM film. As an example, a linear extrapolation at 75.3% RH for the studied film thicknesses is presented in Figure 5. Extrapolated values of the water content per dry mucin for thin and thick PGM layers are similar. The mass ratio of water per dry PGM is independent of the film thickness.

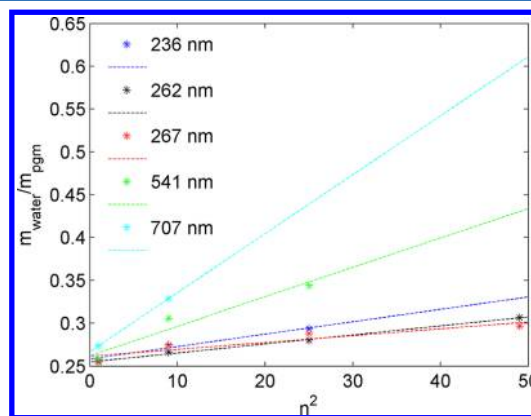


Figure 5. Extrapolation (dashed lines) to the zero overtone for different thicknesses PGM film at 75.3% humidity.

Extrapolated data for a PGM film with thickness of a 267 nm at each RH together with a sorption isotherm obtained by sorption calorimetry¹⁰ are shown in Figure 6a. Extrapolation to the zero overtone gives the true mass of the PGM film at each RH and exhibits good agreement with the sorption calorimetric data.

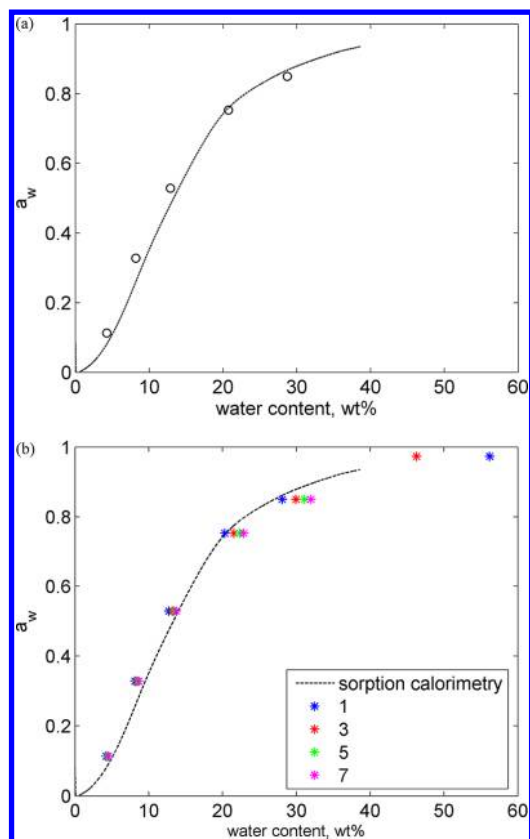


Figure 6. (a) Extrapolated data for PGM film with thickness of 267 nm at each RH from QCM-D experiment (circles) and sorption isotherm obtained by sorption calorimetry¹⁰ (dashed line); (b) Sauerbrey masses of the absorbed water by PGM film obtained by QCM-D and compared with water sorption isotherm studied by sorption calorimetry. Dashed line, sorption calorimetric data;¹⁰ stars, QCM-D data, corresponding to different overtones (blue, 1; red, 3; green, 5; black, 7). The thickness of PGM film is 267 nm.

Sauerbrey masses of the water absorbed by the PGM film obtained by QCM-D were plotted for 1, 3, 5, and 7 overtones and compared with a water sorption isotherm of PGM studied by sorption calorimetry¹⁰ (Figures 6b). Data are presented for a PGM film with the thickness of a 267 nm. Sorption isotherms studied by QCM-D are reproducible at each thickness. Data obtained by two different methods, QCM-D and sorption calorimetry, demonstrate a very good agreement between each other (Figure 6).

Rheological Properties and Glass Transition. Analysis of the overtone dependence on frequency and dissipation changes for the sorption/desorption of a PGM film provides information on the rheological properties of the film. For example, frequency and dissipation changes versus time during sorption/desorption processes for a 267 nm PGM film are presented in Figure 4. It is shown (Figure 4a) that at low RH the overtones are close to each other, then at high RH (52.9–75.3%) overtones start to diverge, and at the highest RH (97.3%) overtones change their order. Dissipation changes ΔD during experiments demonstrate that at low RH there are very small changes in overtone behavior. However, at high RH there are significant changes in dissipation and overtones reverse their order at the highest RH (Figure 4b). Thus, overtone separation and switching of order may indicate the RH levels at which changes of the rheological properties of the PGM film take place. This correlates with the data from our previous work

where it was shown that PGM phase behavior is dependent on hydration levels and the glass transition of mucin system occurs at RH between 60 and 70%.¹⁰

To characterize the changes in rheological properties of mucin during hydration and dehydration, the overtones' dependence on frequency and dissipation shifts were analyzed for each RH level. At the highest RH the overtone behavior is different compared to lower RH levels. Figure 4a shows that the overtones switched their order at the highest humidity, 97.3%. A possible reason can be that the mucin system went through a glass transition,¹⁰ and the PGM film then behaves as a viscous fluid at 97.3% RH. This can be explained using the equation for a semi-infinite viscous liquid³⁴

$$\Delta \tilde{f} = \frac{(i-1)}{\sqrt{2}} \frac{f_0}{\pi Z_q} \sqrt{\rho 2\pi f_0 n \eta} \quad (9)$$

where η is the complex viscosity of the liquid; ρ is the density of the liquid; and $\Delta \tilde{f} = \Delta f + i\Delta\Gamma$ is the shift of the complex resonance frequency. Γ is the bandwidth that can be expressed through dissipation D :

$$\Gamma = \frac{Df}{2} \quad (10)$$

For frequency shifts normalized to the overtone number, one can write

$$\frac{\Delta f}{n} = -\frac{f_0}{Z_q} \sqrt{\frac{f_0 \rho \eta}{\pi n}} \quad (11)$$

where $(\Delta f)/n$ is proportional to $n^{-1/2}$. In other words, the highest overtone should exhibit lowest deviation from zero, which is in agreement with the data for RH level of 97.3% presented in Figure 4a. As an example, the dependence of frequency changes on the overtone number at 97.3% humidity for 236 and 267 nm PGM films are shown in Figure S2 in the Supporting Information. Data on thicker PGM films are not presented because in this case overtones disappeared at the highest RH levels, and only the first overtone was usually left.

At RH levels lower than 97.3%, the normalized frequency shifts either did not depend on the overtone number (the Sauerbrey case, eq 1) or showed a behavior consistent with eq 5, where highest overtones showed the highest deviations from zero. In practice, in QCM-D experiments the overtone behavior was dependent on PGM film thickness. For example, in most of the experiments, when the thicknesses of the PGM films were around 180–370 nm, the overtones were close to each other at low RH levels, started to diverge at 75.3%, and continued to separate at 84.3% RH (Figure 6b). However, for thicker films (thickness higher than 500 nm) the separation of overtones took place at 52.9% RH. With further increase of RH, some overtones disappeared (Figure S3 in the Supporting Information). Based on our previous work,¹⁰ the mucin system undergoes a glass transition, and the RH level for PGM system at which glass transition occurs is between 60 and 70%. According to QCM-D data, possibly the overtone separation takes place at the RH at which the transition of glassy to liquid state of the mucin system occurred. To determine it, the viscoelastic properties of PGM film at RH up to 97.3% were analyzed through the overtone behavior during the frequency changes $(\Delta f)/n$ (eq 8). First, as was mentioned above, data on calculated adsorbed mass were extrapolated to the zero overtones at each RH (Figure 5). This gives the water content

per dry PGM at each RH level. Then the slope and the mass of PGM film, $m_f = m_w + \bar{m}_d$, from extrapolation were used in the following equation

$$b = \frac{\text{the slope}}{m_f^3} \bar{m}_d \quad (12)$$

where b describes the rheological properties of the PGM film since it contains the value of the acoustic impedance of the film, Z_f (eq 5). As a result, the dependence of b versus a_w for different PGM film thicknesses is presented in Figure S4 (Supporting Information). It is observed that b increases with increasing RH. The meaning of this dependence is that the storage modulus, G' , which describes the elasticity of the polymers,³⁵ decreases with increase RH. Hence the solvent, water in this case, starts to act as a plasticizer and softens the PGM film. However, there are no drastic changes in the b plot during the increase of the RH level for each thickness. Instead, the curves look rather smooth. Therefore, it is difficult to determine the exact RH level at which the glass transitions of water–mucin systems occur using only frequency data. To determine the glass transition point, the frequency data should be analyzed together with dissipation data.

The dissipation changes ΔD , in QCM-D measurements, are related to the rheological properties of the studied systems.^{27,36} Therefore, the dissipation changes ΔD were analyzed versus water activity during sorption/desorption processes of PGM film. As an example, a dependence of the normalized dissipation changes on water activity of a 262 nm PGM film is presented in the Figure 7. It is shown that at low RH the

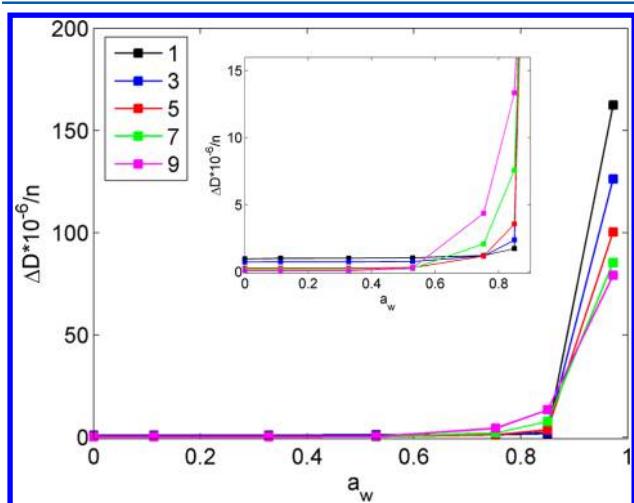


Figure 7. Dependence of the normalized dissipation change on water activity for each overtone of a 262 nm PGM film.

changes in dissipation are close to zero. However, around 52.9% of RH the dissipations start to increase, and at the highest RH level overtones switch their order. Dissipation changes at 97.3% RH are in agreement with data obtained for the frequency changes at the same RH. Thus, dissipation changes can be considered as indicators of changes in the viscoelastic properties of the PGM film. Moreover, those changes occur at similar range of RH as glass transition of the PGM obtained by sorption calorimetry, between 60 and 70% of RH.¹⁰

To study glass transition properties of the PGM film, not only G' but also the loss modulus, G'' , which describes the

viscous properties of the polymers³⁵ should be analyzed. Therefore, the changes in viscoelastic properties of the PGM film can be described using the ratio G'/G'' , which identifies the elastic behavior in relation to the viscous behavior. Viscoelastic properties can be extracted from the equation for a single viscoelastic film in air³⁴

$$\Delta \tilde{f} = -\frac{f_0}{\pi Z_q} Z_f \tan(k_f d_f) \quad (13)$$

where k_f is the wavenumber in the film and d_f is the film thickness. If $k_f d_f$ is much less than unity, the tangent term in eq 13 can be Taylor-expanded to third order as $\tan(x) \approx x + \frac{1}{3}x^3$, resulting in eq 5. An expression for the ratio of the storage modulus to the loss modulus G'/G'' can be derived from eq 5. The full derivation of the ratio G'/G'' (eq 14) can be found in Section SII in the Supporting Information.

Thus, the ratio of the storage modulus to the loss modulus, G'/G'' , can be calculated as

$$\frac{G'}{G''} = -\frac{\Delta f + \frac{2f_0 n m_f}{Z_q}}{\Delta \Gamma} = -\frac{\Delta f + n \left(\frac{\Delta f}{n} \right)_{\text{extrap}}}{\Delta \Gamma} \quad (14)$$

where $(\Delta f/n)_{\text{extrap}}$ is the normalized frequency change extrapolated to the zero overtone. The dependence of G'/G'' over time for overtones 3, 5, and 7 of a 262 nm PGM film is plotted in Figure 8. It is shown that the ratio was very high up

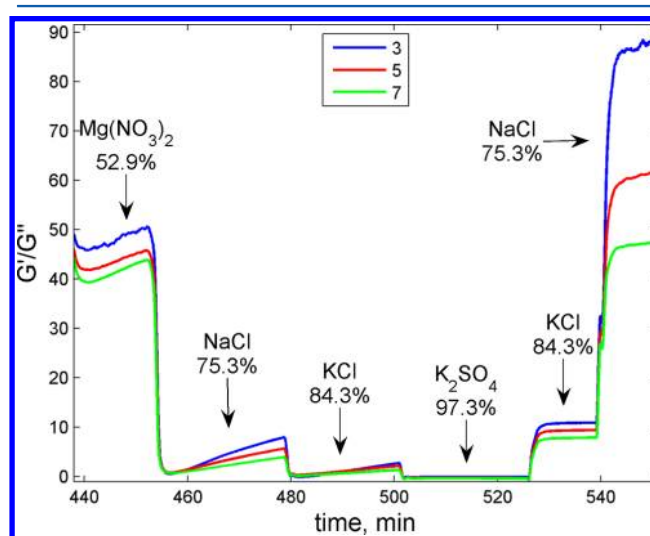


Figure 8. Values of G'/G'' in sorption/desorption experiments with 262 nm PGM film calculated for 3, 5, and 7 overtones.

to 52.9% RH, and at RH values of 75.3, 84.3, and 97.3% the value of G'/G'' is close to zero. Hence the decrease of the storage/loss modulus ratio in sorption process, between 52.9 and 75.3% RH, identifies the glass transition in the mucin film. At high RH the mucin system is more as a liquidlike system and the PGM film behaves as a viscous fluid. The RH levels at which changes in the rheological properties of the PGM film in sorption process obtained by QCM-D take place are in agreement with RH levels at which glass transition in the mucin system as measured by sorption calorimetry occurs around 60–70%.¹⁰ One should note, however, that in the desorption process the glass transition takes place between 75.3 and 84.3% RH. Thus, a sorption/desorption hysteresis in rheological properties of mucin film is observed.

The QCM-D data are in agreement with our previous work on glass transition, showing that this method can be used for studying the glass transition in different systems such as polymer and biopolymer systems. Viscoelastic properties of the studied systems, including glass transition behavior, can be extracted from the QCM-D data without using fitting to models.

4. CONCLUSIONS

Quartz crystal microbalance with dissipation monitoring equipped with a humidity module was used to study hydration/dehydration of pig gastric mucin films. As a prerequisite, adsorption of water on a clean silica sensor was studied. The mucin data were compared to water sorption calorimetric data obtained on the same biopolymer. The following was concluded:

- A good agreement between water sorption isotherms obtained using QCM-D and sorption calorimetry is demonstrated.
- No significant sorption/desorption hysteresis in masses of adsorbed water was observed. However, there is sorption/desorption hysteresis in rheological properties of PGM film.
- The experimentally measured sorption isotherm of pig gastric mucin was not dependent on the thickness of the studied films (within the range of 180–710 nm).
- The QCM-D technique allows studying hydration and rheological properties of relatively thin films and requires less material (only 20–70 μg of PGM is required to obtain a sorption isotherm) and time than those for sorption calorimetry.
- Hydration-induced isothermal glass transition in mucin films was registered using QCM-D. The glass transition occurred in the same humidity range as in the sorption calorimetric experiments.

■ ASSOCIATED CONTENT

Supporting Information

Additional figures and derivations of the equations. This material is available free of charge via the Internet at <http://pubs.acs.org>.

■ AUTHOR INFORMATION

Corresponding Author

*E-mail: vitaly.kocherbitov@mah.se.

Notes

The authors declare no competing financial interest.

[†]On leave from Engelhardt Institute of Molecular Biology RAS, Moscow, Russia.

■ ACKNOWLEDGMENTS

Financial support from Malmo University, the Knowledge Foundation (KK-stiftelsen), and the Gustav Th Ohlsson Foundation is gratefully acknowledged. S.G. acknowledges the Swedish Institute for travel grant.

■ REFERENCES

- (1) Bansil, R.; Turner, B. S. Mucin Structure, Aggregation, Physiological Functions and Biomedical Applications. *Curr. Opin. Colloid Interface Sci.* **2006**, *11*, 164–170.
- (2) Lai, S. K.; Wang, Y. Y.; Wirtz, D.; Hanes, J. Micro- and Macrorheology of Mucus. *Adv. Drug Deliver. Rev.* **2009**, *61*, 86–100.
- (3) Malmsten, M.; Blomberg, E.; Claesson, P.; Carlstedt, I.; Ljusegren, I. Mucin Layers on Hydrophobic Surfaces Studied with

Ellipsometry and Surface Force Measurements. *J. Colloid Interface Sci.* **1992**, *151*, 579–590.

(4) Khanvilkar, K.; Donovan, M. D.; Flanagan, D. R. Drug Transfer through Mucus. *Adv. Drug Delivery Rev.* **2001**, *48*, 173–193.

(5) Davies, J. M.; Viney, C. Water-Mucin Phases: Conditions for Mucus Liquid Crystallinity. *Thermochim. Acta* **1998**, *315*, 39–49.

(6) Sellers, L. A.; Allen, A.; Morris, E. R.; Ross-Murphy, S. B. Mucus Glycoprotein Gels. Role of Glycoprotein Polymeric Structure and Carbohydrate Side-Chains in Gel-Formation. *Carbohydr. Res.* **1988**, *178*, 93–110.

(7) Svensson, O.; Arnebrant, T. Mucin Layers and Multilayers - Physicochemical Properties and Applications. *Curr. Opin. Colloid Interface Sci.* **2010**, *15*, 395–405.

(8) Lafitte, G.; Söderman, O.; Thuresson, K.; Davies, J. Pfg-Nmr Diffusometry: A Tool for Investigating the Structure and Dynamics of Noncommercial Purified Pig Gastric Mucin in a Wide Range of Concentrations. *Biopolymers* **2007**, *86*, 165–175.

(9) Sandberg, T.; Blom, H.; Caldwell, K. D. Potential Use of Mucins as Biomaterial Coatings. I. Fractionation, Characterization, and Model Adsorption of Bovine, Porcine, and Human Mucins. *J. Biomed. Mater. Res. A* **2009**, *91A*, 762–772.

(10) Znamenskaya, Y.; Sotres, J.; Engblom, J.; Arnebrant, T.; Kocherbitov, V. Effect of Hydration on Structural and Thermodynamic Properties of Pig Gastric and Bovine Submaxillary Gland Mucins. *J. Phys. Chem. B* **2012**, *116*, 5047–5055.

(11) Yakubov, G. E.; Papagiannopoulos, A.; Rat, E.; Easton, R. L.; Waigh, T. A. Molecular Structure and Rheological Properties of Short-Side-Chain Heavily Glycosylated Porcine Stomach Mucin. *Biomacromolecules* **2007**, *8*, 3467–3477.

(12) Di Cola, E.; Yakubov, G. E.; Waigh, T. A. Double-Globular Structure of Porcine Stomach Mucin: A Small-Angle X-Ray Scattering Study. *Biomacromolecules* **2008**, *9*, 3216–3222.

(13) Momoh, M. A.; Adikwu, M. U.; Ibezim, C. E.; Ofokansi, K. C.; Attama, A. A. Thermal Characterisation of Pegylated Mucin. *Asian Pac. J. Trop. Med.* **2010**, *3*, 458–460.

(14) Patel, M. M.; Smart, J. D.; Nevell, T. G.; Ewen, R. J.; Eaton, P. J.; Tsiabouklis, J. Mucin/Poly(Acrylic Acid) Interactions: A Spectroscopic Investigation of Mucoadhesion. *Biomacromolecules* **2003**, *4*, 1184–1190.

(15) Viney, C. Mucus Liquid Crystallinity: Is Function Related to Microstructural Domain Size? *Biorheology* **1999**, *36*, 319–323.

(16) Viney, C.; Huber, A. E.; Verdugo, P. Liquid-Crystalline Order in Mucus. *Macromolecules* **1993**, *26*, 852–855.

(17) Waigh, T. A.; Papagiannopoulos, A.; Voice, A.; Bansil, R.; Unwin, A. P.; Dewhurst, C. D.; Turner, B.; Afdhal, N. Entanglement Coupling in Porcine Stomach Mucin. *Langmuir* **2002**, *18*, 7188–7195.

(18) Builders, P. F.; Kunle, O. O.; Adikwu, M. U. Preparation and Characterization of Mucinated Agarose: A Mucin-Agarose Physical Crosslink. *Int. J. Pharm.* **2008**, *356*, 174–180.

(19) Krtil, P.; Trojanek, A.; Samec, Z. Kinetics of Water Sorption in Nafionthion Films - Quartz Crystal Microbalance Study. *J. Phys. Chem. B* **2001**, *105*, 7979–7983.

(20) Yamamoto, Y.; Ferrari, M. C.; Baschetti, M. G.; De Angelis, M. G.; Sarti, G. C. A Quartz Crystal Microbalance Study of Water Vapor Sorption in a Short Side-Chain Ppsi Membrane. *Desalination* **2006**, *200*, 636–638.

(21) Lubarsky, G. V.; Davidson, M. R.; Bradley, R. H. Hydration-Dehydration of Adsorbed Protein Films Studied by Afm and Qcm-D. *Biosens. Bioelectron.* **2007**, *22*, 1275–1281.

(22) Smith, A. L.; Shirazi, H. M.; Mulligan, S. R. Water Sorption Isotherms and Enthalpies of Water Sorption by Lysozyme Using the Quartz Crystal Microbalance/Heat Conduction Calorimeter. *BBA—Protein Struct. Mol. Enzymol.* **2002**, *1594*, 150–159.

(23) Okur, S.; Kus, M.; Ozel, F.; Yilmaz, M. Humidity Adsorption Kinetics of Water Soluble Calix[4]Arene Derivatives Measured Using Qcm Technique. *Sensors Actuators B—Chem.* **2010**, *145*, 93–97.

(24) Russell, S. P.; Weinkauff, D. H. Vapor Sorption in Plasma Polymerized Vinyl Acetate and Methyl Methacrylate Thin Films. *Polymer* **2001**, *42*, 2827–2836.

- (25) D'Arcy, R. L.; Watt, I. C. Analysis of Sorption Isotherms of Non-Homogeneous Sorbents. *Trans. Faraday Soc.* **1970**, *66*, 11236–11245.
- (26) Greenspan, L. Humidity Fixed Points of Binary Saturated Aqueous Solutions. *J. Res. Natl. Bur. Stand. Sect. A* **1977**, *81*, 89–96.
- (27) Rodahl, M.; Kasemo, B. A Simple Setup to Simultaneously Measure the Resonant Frequency and the Absolute Dissipation Factor of a Quartz Crystal Microbalance. *Rev. Sci. Instrum.* **1996**, *67*, 3238–3241.
- (28) Halthur, T. J.; Arnebrant, T.; Macakova, L.; Feiler, A. Sequential Adsorption of Bovine Mucin and Lactoperoxidase to Various Substrates Studied with Quartz Crystal Microbalance with Dissipation. *Langmuir* **2010**, *26*, 4901–4908.
- (29) Horcas, I.; Fernandez, R.; Gomez-Rodriguez, J. M.; Colchero, J.; Gomez-Herrero, J.; Baro, A. M. Wsxn: A Software for Scanning Probe Microscopy and a Tool for Nanotechnology. *Rev. Sci. Instrum.* **2007**, *78*.
- (30) Sotres, J.; Barrantes, A.; Arnebrant, T. Friction Force Spectroscopy as a Tool to Study the Strength and Lateral Diffusion of Protein Layers. *Langmuir* **2011**, *27*, 9439–9448.
- (31) Sauerbrey, G. Verwendung Von Schwingquarzen Zur Wägung Dünner Schichten Und Zur Mikrowägung. *Z. Phys. A Hadrons Nuclei* **1959**, *155*, 206–222.
- (32) Kocherbitov, V.; Alfredsson, V. Assessment of Porosities of Sba-15 and Mcm-41 Using Water Sorption Calorimetry. *Langmuir* **2011**, *27*, 3889–3897.
- (33) Sotres, J.; Baro, A. M. AFM Imaging and Analysis of Electrostatic Double Layer Forces on Single DNA Molecules. *Biophys. J.* **2010**, *98*, 1995–2004.
- (34) Johannsmann, D. Viscoelastic Analysis of Organic Thin Films on Quartz Resonators. *Macromol. Chem. Phys.* **1999**, *200*, 501–516.
- (35) Oertel, R.; Kulicke, W. M. Viscoelastic Properties of Liquid Crystals of Aqueous Biopolymer Solutions. *Rheol. Acta* **1991**, *30*, 140–150.
- (36) Rodahl, M.; Hook, F.; Krozer, A.; Brzezinski, P.; Kasemo, B. Quartz-Crystal Microbalance Setup for Frequency and Q-Factor Measurements in Gaseous and Liquid Environments. *Rev. Sci. Instrum.* **1995**, *66*, 3924–3930.